Transportation Research Part C 72 (2016) 306–324

Contents lists available at ScienceDirect

Transportation Research Part C

journal homepage: www.elsevier.com/locate/trc

Driving safety field theory modeling and its application in pre-collision warning system

Jianqiang Wang [a,*], Jian Wu [a], Xunjia Zheng [a], Daiheng Ni [b], Keqiang Li [a,*]

[a] State Key Laboratory of Automotive Safety and Energy, Tsinghua University, Beijing 100084, China
[b] University of Massachusetts, Amherst, MA 01003, United States

ARTICLE INFO

Article history:
Received 17 December 2015
Received in revised form 23 September 2016
Accepted 4 October 2016
Available online 14 October 2016

Keywords:
Driving safety field
Pre-collision warning
Intelligent vehicle
Driving risk estimation
Driver–vehicle–road interactions
Driver assistance system

ABSTRACT

The concept and contents of driving safety field theory were presented in our previous study. On this basis, this study focus on driving safety field theory modeling and application. First, a general model is presented, which considered the driver-vehicle-road interactions. The model include the following three parts: (i) driver behaviors, which are determined by driver characteristics, such as physical-psychological, cognition, driving skill, and traffic violations; (ii) vehicle characteristics, which are determined by velocity vectors and virtual masses of vehicles; (iii) road conditions, which are determined by virtual mass of on road non-moving objects, types of traffic signs, road adhesion coefficient, road slope, road curvature, and visibility. In order to establish concrete functional forms, the specific model is presented. This specific model provides a method for virtual mass calculation and describes the field strength and field force in detail. After that, a driving safety indicator namely DSI is defined. Finally, a vehicle collision warning algorithm based on driving safety field model is presented. This algorithm used a new index namely RDSI to evaluate the driving risk level. The effectiveness of this collision warning algorithm is verified by field experiments.

1. Introduction

Advanced driver assistance systems (ADAS) have played an important role in improving driving safety. Since the 1990s, automotive companies have been proposing and applying several driving safety assistance algorithms to their driver safety assistance products. However, these algorithms were fairly simplistic. For longitudinal safety, in particular, the safety distance model is used to describe a vehicle's safety state. When the following distance between leading and following vehicles is less than the safety distance, the assistance system sounds an alarm and engages the brake on the following vehicle. Many safety distance models determine the vehicle's safety state by analyzing the safety distance between leading and following vehicles during relative movement (Abdel-Aty et al., 2006; Caliendo et al., 2007). Time to collision (TTC) (Kiefer et al., 2006) and time headway (THW) (Yiğiter et al., 2014) have been widely used as parameters for measuring the longitudinal driving risk. For lateral safety, driver safety assistance algorithms are based mainly on a car's current position (CCP) (Heddebaut et al., 2005), time-to-lane cross (TLC) (Mammar et al., 2006), and variable rumble strip (VRBS) (Pilutti and Ulsoy, 2003). The existing safety models are based mainly on vehicle kinematics and dynamics, and their descriptions of vehicle driving safety are generally based on information of the vehicle's state, such as position, velocity, acceleration, and yaw velocity, in

* Corresponding authors.
E-mail addresses: wjqlws@tsinghua.edu.cn (J. Wang), likq@tsinghua.edu.cn (K. Li).

http://dx.doi.org/10.1016/j.trc.2016.10.003
0968-090X/

addition to information about the vehicle's relative movement, relative velocity, and relative distance. However, it is difficult for these models to reflect the effects of a greater number of traffic factors on driving safety, describe interactions among driver behavior characteristics, vehicle states, and road environment, or provide accurate judgment bases for vehicle control. On the basis of the risk homeostasis theory (RHT) and the stimulus-response concept, Lu et al. (2012, 2013) proposed a desired safety margin (DSM) model, which serves as a new way to explain car following. In addition, the drivability maps method was well applied in the researches of intelligent vehicle control (Neuhaus et al., 2009; Tawari et al., 2014; Schwarz and Behnke, 2014). In order to estimate the risk effects of distracted driving, Przybyla et al. (2015) incorporated a dynamic, data-driven car-following model in an algorithmic framework. Similarly, M. Wang et al. (2015) presented an approach to generate optimal lane change decisions in the predicted future, including strategic overtaking, cooperative merging and selection of a safe gap. On the other hand, artificial potential field theory have been widely used for motion planning and collision avoidance for automated vehicles and robots. The first application of artificial potential field for mobile robot obstacle avoidance was by Khatib (1986), he proposed the virtual obstacle concept to escape local minimums in local path planning based on artificial potential field approach. Over the following decade, artificial potential field theory was widely used in mobile robot path planning (Warren, 1990; Rimon and Koditschek, 1992; Kitamura et al., 1995; Veelaert and Bogaerts, 1999), in the meanwhile, intelligent transport system have been promoted rapidly (Van Der Laan et al., 1997; Bourhis et al., 2001; Cui and Ge, 2003; Li et al., 2004; Beard et al., 2005). Because the advantage of the artificial potential field, some researchers used it to study the autonomous vehicle control. Rossetter and Gerdes (2006) proposed a method by which an energy term consisting of the vehicle's kinetic energy and the artificial potential energy can be bounded, leading to a bound on lateral deviation; instead of, this method is only applicable to lane-keeping scenarios. In the last decade, the ITS technologies developed rapidly, and the applications of artificial potential field theory become more and more mature and widespread. Pengfei et al. (2011) improved the simulation accuracy of car-following model and describing the characteristics of car-following driving behavior by using artificial potential field theory. In order to reduce the risk of vehicle collision, some researchers put their focus on right-turning traffic collision scenarios (Dabbour and Easa, 2014) or general traffic scenarios (Ward et al., 2015). Moreover, artificial potential theory is beneficial for transportation research (Jacob and Abdulhai, 2010; Suzuki et al., 2010). In 2013, Raksincharoensak et al. (2013) proposed a braking assistance system algorithm for collision avoidance, designed based on pedestrian motion prediction and risk potential. Recently, Ni (2013) introduced a Field Theory with an emphasis on traffic flow modeling at the microscopic level. In this theory, highways and vehicles were perceived as a field by a driver whose driving strategy is to navigate through the field along its valley. Similarly, Jian et al. (2014) proposed a perceived potential field and an aggregated force field for navigation of pedestrians in a walking domain with poor visibility or complex geometries, but this research mainly focuses on the pedestrian. To better adapt safety algorithms to driver behavior, an algorithm that autonomously learns driver characteristics was proposed by researchers at Tsinghua University based on the recursive least-square method with a forgetting factor; this algorithm was used in an adaptive longitudinal driver assistance system (Wang et al., 2013). However, there are some drawbacks to the existing safety-assistance methods. Firstly, only a limited number of driving safety influence factors and their effects are considered. Secondly, most applications of these methods are limited to simple scenarios. Furthermore, these methods are difficult to adapt to increasingly complex traffic environments, particularly the vehicle kinematics- and dynamics-based methods.

Recently, a new research method for driving safety, called the driving safety field, was proposed (J. Wang et al., 2014, 2015). This method uses field theory to represent the driving risk due to various traffic factors, and it could be used to evaluate potential driving risk in real traffic scenarios. In this study, we formulated a general model of the driving safety field and proposed a novel vehicle collision warning algorithm based on the driving safety field. This algorithm overcomes some of the aforementioned drawbacks, and can be applied to multi-vehicle scenarios.

The rest of this paper is arranged as follows. In Section 2, the new concept and modified general model of the driving safety field is described briefly. In Section 3, a specific model of driving safety field is proposed. In Section 4, a vehicle collision warning algorithm is designed based on the specific driving safety field model. In Section 5, three experimental vehicles are introduced and field experiments are described. The vehicle collision warning algorithm is verified by applying it in a typical car-following scenario on a multi-lane road. Section 6 presents the discussions of this study. Section 7 presents the conclusions of this study.

2. General model of driving safety field

In this section, the driving safety field concept is introduced. Based on J. Wang et al. (2014, 2015), the driving safety field model comprises the potential, kinetic, and behavior fields, $\boldsymbol{E}_S$, $\boldsymbol{E}_R$, $\boldsymbol{E}_V$, and $\boldsymbol{E}_D$ denoting the field strength vectors of the driving safety field, potential field, kinetic field, and behavior field, respectively, the driving safety field model can be expressed as

$$\boldsymbol{E}_S = \boldsymbol{E}_R + \boldsymbol{E}_V + \boldsymbol{E}_D \tag{1}$$

The field strength vectors in (1) describe the potential driving risks due to traffic factors in actual scenarios. The risk is measured by the possibility of an accident and the severity of such an accident. For non-moving objects of the first category, according to the above analysis, the field strength vector $\boldsymbol{E}_{R1,aj}$ at (x_j, y_j) in the potential field formed by a non-moving object a at (x_a, y_a) on the road is

$$\boldsymbol{E}_{R1,aj} = \boldsymbol{E}_{R1,aj}(R_a, M_a, \boldsymbol{r}_{aj}) \tag{2}$$

where M_a is the virtual mass of object a, and R_a is the road condition influencing factor at (x_a, y_a), $\boldsymbol{r}_{aj} = (x_j - x_a, y_j - y_a)$ is the distance vector.

For non-moving objects of the second category, the lane marker model was employed. As Fig. 1 shows, the field strength vector $\boldsymbol{E}_{R2,aj}$ at (x_a, y_a) of the potential field owing to lane marker a is

$$\boldsymbol{E}_{R2,aj} = \boldsymbol{E}_{R2,aj}(LT_a, R_a, D, \boldsymbol{r}_{aj}) \tag{3}$$

where LT_a is the type of lane marker a, which is determined by local traffic laws and regulations, for example, the value of lane marker 1 (white solid line) is larger than that of lane marker 2 (white dotted line); D is the lane width; $\boldsymbol{r}_{aj} = (x_j - x_a, y_j - y_a)$ is the distance vector between lane marker a and the center of mass of the vehicle (which is shown as a white rectangle in Fig. 1.

M_i is used to measure the potential driving risk due to the attributes of object i. Here, the potential driving risk mainly refers to potential losses due to a collision between object i and a vehicle. This risk is associated with the attributes of the object, such as its mass, type, moving state, and, in particular, speed. The virtual mass M_i of object i is defined as

$$M_i = M_i(m_i, T_i, v_i) \tag{4}$$

where m_i is the actual physical mass, T_i is the type, and v_i is the velocity of object i. Moreover, object i can be either non-moving or moving.

R_i is used to indicate the potential driving risk due to the road conditions at (x_i, y_i). Here, the potential driving risk refers mainly to both the possibility and severity of a collision between object i and a vehicle. These road conditions include the road adhesion coefficient, road slope, road curvature, and visibility. R_i, the influencing factor pertaining to road conditions at (x_i, y_i), is defined as

$$R_i = R_i(\delta_i, \mu_i, \rho_i, \tau_i) = \Psi_\delta(\delta_i) \cdot \Psi_\mu(\mu_i) \cdot \Psi_\rho(\rho_i) \cdot \Psi_\tau(\tau_i) \tag{5}$$

where δ_i is the visibility, μ_i is the road adhesion coefficient, ρ_i is the road curvature, and τ_i is the slope of the road at the position of object i. Ψ_δ, Ψ_μ, Ψ_ρ, Ψ_τ express the risk evaluation functions of δ_i, μ_i, ρ_i, τ_i, respectively.

The kinetic field is a physical field that denotes the influence of moving objects on driving safety. Here, moving objects refer to those that can actually collide with vehicles and cause significant losses. The field strength vector $\boldsymbol{E}_{V,bj}$ at (x_j, y_j) of the kinetic field formed by a moving object b at (x_b, y_b) on the road is

$$\boldsymbol{E}_{V,bj} = \boldsymbol{E}_{V,bj}(R_b, M_b, \boldsymbol{r}_{bj}, \boldsymbol{v}_b) \tag{6}$$

where $\boldsymbol{v}_b$ is the velocity vector of object b. $\boldsymbol{E}_{V,bj}$ is directed along the gradient descent direction of the field strength, which is also away from object b.

The behavior field is a physical field that denotes the influence of driver behavior characteristics on driving safety. The field strength vector $\boldsymbol{E}_{D,cj}$ at (x_j, y_j) in the behavior field formed by the driver of vehicle c (not the controlling vehicle) at (x_c, y_c) is

$$\boldsymbol{E}_{D,cj} = \boldsymbol{E}_{V,cj} \cdot DR_c = \boldsymbol{E}_{V,cj} \cdot (\omega_1 \cdot DR_{p,c} + \omega_2 \cdot DR_{c,c} + \omega_3 \cdot DR_{s,c} + \omega_4 \cdot DR_{v,c}) \tag{7}$$

where DR_c is the driver risk factor associated with the driver of vehicle c, and $\boldsymbol{E}_{V,cj}$ is the field strength vector of the kinetic field formed by vehicle c. $DR_{p,c}$, $DR_{c,c}$, $DR_{s,c}$, $DR_{v,c}$ express the risk factors of physical-psychological, cognition, driving skill, and traffic violations, respectively. The driver risk factor DR_c is a dimensionless value between 0 and 1 that is determined according to the driver's performance in the above four aspects, and the $\omega_i (i = 1, 2, 3, 4,)$ is the weight coefficient.

(1) Field force on vehicle: A vehicle in the driving safety field, which includes the three aforementioned fields, experiences a field force that denotes the current driving risk associated with the vehicle. The field strength vector, road conditions at the vehicle's location, vehicle's attributes, and driver's behavior characteristics determine the field force acting on the vehicle. Consider the driving safety field formed by object i. In this field, the field force on the vehicle j at (x_j, y_j) is

$$\boldsymbol{F}_{ij} = \boldsymbol{F}(\boldsymbol{E}_{ij}, M_j, R_j, DR_j) \tag{8}$$

where $\boldsymbol{E}_{ij}$ is the field strength vector of the driving safety field at (x_j, y_j), and $\boldsymbol{F}_{ij}$ is the field force.

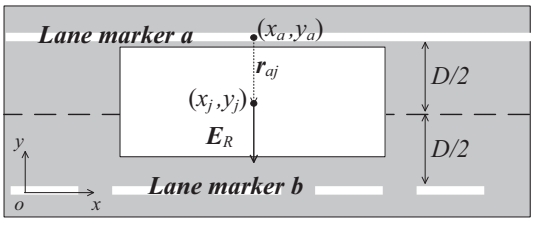

Fig. 1. Diagram of lane marker model.

The field force can be a good indicator of the magnitude and direction of driving risk due to a single object. However, the resultant force, which is the vector sum of field forces, does not reflect the combined driving risk due to multiple objects. This is because forces are vectors and opposite vectors cancel each other, but the driving risk would only increase without counteraction. Therefore, vectors do not reflect the combined driving risk, and a scalar is needed to denote the combined driving risk when a vehicle is influenced by multiple objects.

(2) Safety potential energy and its change rate with time: As mentioned previously, the driving safety field formed by object i is a vector field. A vehicle j in this field is acted upon by field force $\boldsymbol{F}_{ij}$, and the direction of $\boldsymbol{F}_{ij}$ is the same as that of $\boldsymbol{E}_{ij}$, which is the gradient descent direction of $\boldsymbol{E}_{ij}$, such that $\boldsymbol{F}_{ij} = |\boldsymbol{F}_{ij}|(-\nabla \boldsymbol{E}_{ij}/|\nabla \boldsymbol{E}_{ij}|)$. Based on this, we can calculate the curl of $\boldsymbol{F}_{ij}$ as

$$\begin{aligned}\operatorname{curl} \boldsymbol{F}_{ij} &= \nabla \times \boldsymbol{F}_{ij} \\ &= \nabla \times \left(|\boldsymbol{F}_{ij}| \frac{-\nabla \boldsymbol{E}_{ij}}{|\nabla \boldsymbol{E}_{ij}|} \right) \\ &= -\frac{|\boldsymbol{F}_{ij}|}{|\nabla \boldsymbol{E}_{ij}|} \left[\nabla \times \left(\frac{\partial |\boldsymbol{E}_{ij}|}{\partial x} \boldsymbol{i} + \frac{\partial |\boldsymbol{E}_{ij}|}{\partial y} \boldsymbol{j} \right) \right] \\ &= -\frac{|\boldsymbol{E}_{ij}|}{|\nabla \boldsymbol{E}_{ij}|} \left(\frac{\partial^2 |\boldsymbol{E}_{ij}|}{\partial x \partial y} - \frac{\partial^2 |\boldsymbol{E}_{ij}|}{\partial y \partial x} \right) \\ &= 0\end{aligned} \tag{9}$$

Therefore, the driving safety field formed by object i is a conservative vector field (or an irrotational field).

For such a conservative vector field, there exists a scalar potential, whose gradient is the field force. We denote this scalar potential as safety potential energy (SPE), which is the energy that a vehicle has due to the conservative field force acting on it in a driving safety field. Taking as an example the driving safety field formed by object i, after defining the safety potential energy of vehicle j as zero when the distance between vehicle j and object i is infinite in this driving safety field, we can obtain the safety potential energy of vehicle j as

$$\mathrm{SPE}_{ij} = -\int_{\infty}^{\boldsymbol{r}_{ij}} \boldsymbol{F}_{ij} \cdot d\boldsymbol{r} \tag{10}$$

where SPE_{ij} is the safety potential energy of vehicle j in the driving safety field formed by object i, and $\boldsymbol{r}_{ij}$ is the distance vector between vehicle j and object i. As mentioned previously, $\boldsymbol{F}_{ij}$ is a repulsive force. Therefore, SPE_{ij}, the calculation result of (10), is positive. SPE_{ij} is decided by the position of vehicle j, and it reflects the distribution of driving risk in space. A large SPE_{ij} value reflects high risk.

Moreover, the driving risk varies not only with space but also with time. However, the safety potential energy represents only the spatial variability of driving risk. Therefore, another physical index is necessary to denote the temporal variability of driving risk. In this paper, the change rate of safety potential energy with time ($\dot{\mathrm{SPE}} = \frac{d\mathrm{SPE}}{dt}$) is used as this index. For SPE_{ij}, its change rate with time is

$$\dot{\mathrm{SPE}}_{ij} = \frac{d\mathrm{SPE}}{dt} = \frac{d\mathrm{SPE}}{d\boldsymbol{r}} \cdot \frac{d\boldsymbol{r}}{dt} = -\boldsymbol{F}_{ij} \cdot \frac{d\boldsymbol{r}}{dt} = \boldsymbol{F}_{ij} \cdot (\boldsymbol{v}_i - \boldsymbol{v}_j) \tag{11}$$

A positive $\dot{\mathrm{SPE}}_{ij}$ reflects an increasing SPE_{ij}, namely increasing risk to vehicle j due to object i.

The individual safety potential energy and its change rate with time have been defined as above. However, to obtain the total safety potential energy and its temporal rate of change, simply adding the individual energy values is inadequate. This is because the weights of the safety potential energies due to objects in different lanes are not equal. For example, for vehicle j, the vehicle in the same lane may have greater influence than another vehicle in the adjacent lane. Meanwhile, for vehicle j, the lateral position of the vehicle in the adjacent lane and lane width are two crucial factors that determine the weight. Here, we explicate this phenomenon as the filtering effects of lane markers.

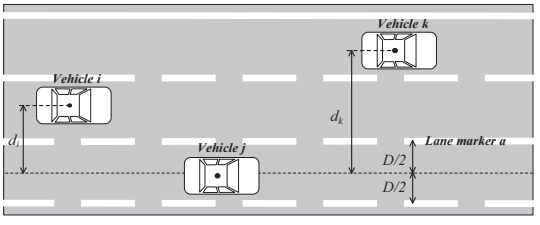

Fig. 2. Multi-lane scenario.

Additional details are given in the following case. A multi-lane scenario is shown in Fig. 2, in which three vehicles are driving in three lanes (vehicle i in the middle lane, vehicle j in the right lane, and vehicle k in the left lane). d_i(or d_k) is the lateral distance between the mass center of vehicle i (or vehicle k) and the centerline of the right lane. In this case, vehicle j is influenced by two driving safety fields formed by vehicle i and vehicle k. The total safety potential energy of vehicle j (SPE_j) is calculated as

$$\begin{cases} \mathrm{SPE}_j = h_i \cdot SPE_{ij} + h_k \cdot SPE_{kj} \\ h_i = h(d_i, D) \\ h_k = h(d_k, D) \end{cases} \tag{12}$$

where $h_i (0 < h_i \leqslant 1)$ and $h_k (0 < h_k \leqslant 1)$ are the weights of SPE_{ij} and SPE_{kj}, respectively, which represent the filtering effects of lane marker a. h_i increases with a decrease in d_i. Especially when $d_i \leqslant D/2$, $h_i = 1$. As (12) shows, lane marker a reduces the influence of vehicles in other lanes on the driving safety of vehicle j.

(3) Driving safety index: Based on the safety potential energy and its temporal change rate, an integrated index called the driving safety index (DSI) is proposed to denote the driving risk to a vehicle, which varies spatially and temporally. The driving safety index of vehicle j is defined as

$$\mathrm{DSI}_j = \mathrm{DSI}(\mathrm{SPE}_j, \dot{\mathrm{SPE}}_j) \tag{13}$$

where DSI_j, a dimensionless quantity, is the driving safety index of vehicle j. A large DSI_j value reflects high driving risk to vehicle j.

(4) Unified model of driving safety field: In summary, the unified model of the driving safety field is

$$\begin{cases} \mathrm{SPE}_j = \mathrm{SPE}_{R,j} + \mathrm{SPE}_{V,j} + \mathrm{SPE}_{D,j} \\ \qquad = \sum_a (h_a \cdot \mathrm{SPE}_{R,aj}) + \sum_b (h_b \cdot \mathrm{SPE}_{V,bj}) + \sum_c (h_c \cdot \mathrm{SPE}_{D,cj}) \\ \dot{\mathrm{SPE}}_j = \sum_a (h_a \cdot \dot{\mathrm{SPE}}_{R,aj}) + \sum_b (h_b \cdot \dot{\mathrm{SPE}}_{V,bj}) + \sum_c (h_c \cdot \dot{\mathrm{SPE}}_{D,cj}) \\ \qquad = -\sum_a (h_a \cdot \boldsymbol{F}_{aj} \cdot \boldsymbol{v}_j) + \sum_b [h_b \cdot \boldsymbol{F}_{bj} \cdot (\boldsymbol{v}_b - \boldsymbol{v}_j)] + \sum_c [h_c \cdot \boldsymbol{F}_{cj} \cdot (\boldsymbol{v}_c - \boldsymbol{v}_j)] \\ \mathrm{DSI}_j = \mathrm{DSI}(\mathrm{SPE}_j, \dot{\mathrm{SPE}}_j) \end{cases} \tag{14}$$

where $\mathrm{SPE}_{R,j}$, $\mathrm{SPE}_{V,j}$, and $\mathrm{SPE}_{D,j}$ are respectively the total safety potential energies of vehicle j in the potential field, kinetic field, and behavior field; $\mathrm{SPE}_{R,aj}$, $\mathrm{SPE}_{V,bj}$, and $\mathrm{SPE}_{D,cj}$ are respectively the safety potential energies of vehicle j in the individual potential field, kinetic field, and behavior field; and $\boldsymbol{F}_{aj}$, $\boldsymbol{F}_{bj}$, and $\boldsymbol{F}_{cj}$ are respectively the field forces on vehicle j in the individual potential field, kinetic field, and behavior field.

3. Specific model of driving safety field

In Section 2, the general theory of driving safety field was introduced. Without loss of generality, the exact functional forms of the formulas were not given. In this section, based on our previous research and by learning from physical theories, we proposed a specific model of the driving safety field in which the exact functional forms of the formulas are discussed.

3.1. Virtual mass

Virtual mass M_i is used to measure the potential driving risk due to the attributes (mass, type, and speed) of object i, and the potential driving risk mainly refers to potential losses due to a collision between object i and a vehicle. For objects of the same type, a greater physical mass and speed of the object reflect larger virtual mass and higher potential losses. Moreover, with the same physical mass and speed, the potential loss due to a collision depends on the object type. For example, the loss due to a collision between a pedestrian and a vehicle is larger than that due to a collision between an animal and a vehicle. Therefore, the specific from of M_i can be defined as

$$M_i = M_i(m_i, T_i, v_i) = m_i \cdot T_i \cdot g(v_i) \tag{15}$$

where $g(v_i)$ is a function of speed that is used to describe the influence of speed on driving risk. The calibration of $g(v_i)$ can be implemented based on accident data.

Table 1 lists the road speeds and numbers of accidents of five main types of roads in China, 2013 (Transportation Bureau of the Ministry of Public Security of the PRC, 2014). As shown in Fig. 3, by fitting the average number of fatalities per accident as a power function of average road speed, we obtain

$$num = 1.566 \times 10^{-14} v^{6.687} + 0.3345 \tag{16}$$

where num is the average number of fatalities per accident and v (km/h) is the average road speed.

Table 1
Road speed and accidents in China, 2013.

Road	Design speed [km/h]	Average speed [km/h]	Number of accidents	Number of fatalities	Average number of fatalities
Highway	80–120	100	8693	5843	0.672
First-class road	60–80	70	18,198	6532	0.359
Second-class road	40–60	50	36,556	13,642	0.373
Third-class road	30–40	35	22,936	7499	0.327
Fourth-class road	30	30	15,956	5006	0.314

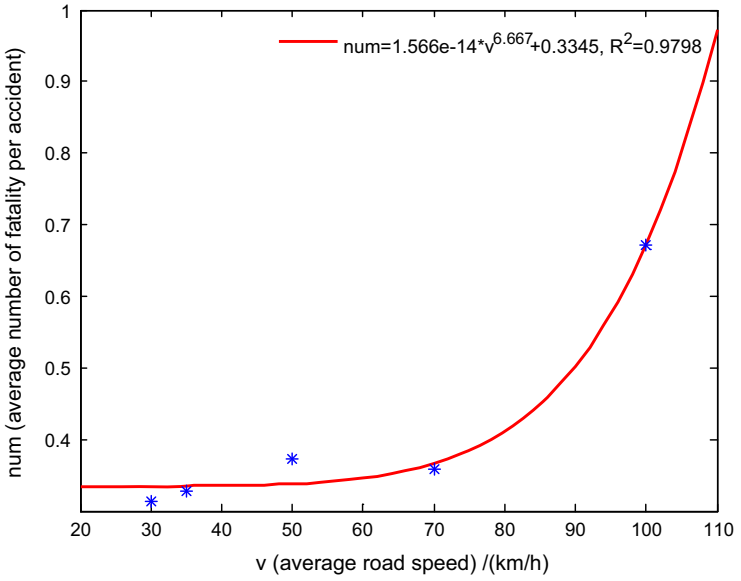

Fig. 3. Relationship between average road speed and average number of fatalities per accident.

Hence, $g(v_i)$ can be determined using the above formula. Finally, we obtain

$$M_i = m_i \cdot T_i \cdot (1.566 \times 10^{-14} v_i^{6.687} + 0.3345) \tag{17}$$

3.2. Field strength and field force

Based on the features of driving risk due to non-moving objects of the first category and by making analogy to electric field, we express the field strength vector of such objects as:

$$\boldsymbol{E}_{R1,aj} = \boldsymbol{E}_{R1,aj}(R_a, M_a, \boldsymbol{r}_{aj}) = \frac{K \cdot R_a \cdot M_a}{|\boldsymbol{r}_{aj}|^{k_1}} \cdot \frac{\boldsymbol{r}_{aj}}{|\boldsymbol{r}_{aj}|} \tag{18}$$

where K (>0) and k_1 (>1) are undetermined constants. The direction of $\boldsymbol{E}_{R1,aj}$ is the same as that of $\boldsymbol{r}_{aj}$, which is the gradient descent direction of the field strength.

Based on the features of driving risk due to non-moving objects of the second category (only lane marker is considered at present) and using the spring model as a analogy, the field strength vector of such objects can be expressed as

$$\boldsymbol{E}_{R2,aj} = \boldsymbol{E}_{R,L}(LT_a, R_a, D, \boldsymbol{r}_{aj}) = LT_a \cdot R_a \cdot \left(\frac{D}{2} - |\boldsymbol{r}_{aj}|\right)^{k_2} \cdot \frac{\boldsymbol{r}_{aj}}{|\boldsymbol{r}_{aj}|} \tag{19}$$

where k_2 is an undetermined constant greater than zero.

Compared with first-class stationary objects, the main difference is that the driving risk due to moving objects changes with direction; when the distance is the same, driving risk to the vehicle will be larger when approaching the direction of motion of a moving object. Here, the Doppler effect is used to describe the differences among the driving risks in each direction, which are caused by movement. The moving object b is considered to launch a wave of frequency f_0, and the receiver at location (x_j, y_j) receives a wave of frequency f_1. The higher the frequency of the received wave, the larger the influence of the moving object b at this location will be. According to the Doppler Effect, we obtain

$$\frac{f_1}{f_0} = \frac{k_3}{k_3 - |\boldsymbol{v}_b| \cos\theta_b} \tag{20}$$

where k_3 is the speed of the wave, and θ_b is the angle between v_b and r_{ij} (clockwise is positive). The frequency of the wave increases as the distance between the wave propagation direction and the direction of motion of the object decreases. This is similar to the differences among driving risks in each direction due to movement. The variation of frequency can be used to describe the influence of vehicle speed on driving risk. Hence, combined with potential field model, the strength of the kinetic field can be expressed as

$$\boldsymbol{E}_{V,bj} = \boldsymbol{E}_V(R_b, M_b, \boldsymbol{r}_{bj}, \boldsymbol{v}_b) = \frac{K \cdot R_b \cdot M_b \cdot k_3}{(k_3 - |\boldsymbol{v}_b| \cos\theta_b) \cdot |\boldsymbol{r}_{bj}|^{k_1}} \cdot \frac{-\nabla \boldsymbol{E}_{V,bj}}{|\nabla \boldsymbol{E}_{V,bj}|} \tag{21}$$

where $\nabla \boldsymbol{E}_{V,bj}$ is the gradient vector of $\boldsymbol{E}_{V,bj}$, and the direction of $\boldsymbol{E}_{V,bj}$ is the same as the gradient descent direction of the field strength. Therefore, according to (7) and (21), the specific strength of the behavior field can be obtained (see Figs. 4 through 6).

The kinetic field strength in (21) is shown in Fig. 7. The center of the kinetic field is the object's center of mass. Contrary to the behavior of the potential field formed by a nonmoving object, at an equivalent distance, the field strength increases as the angle between the direction of motion of the object ($\boldsymbol{v}_b$) and the direction of $\boldsymbol{r}_{bj}$ decreases. In addition, multiple moving objects and the field strength of their corresponding kinetic fields are shown in Fig. 8, and the field strength of multi-vehicle scenarios and their corresponding driving safety fields are shown in Fig. 9.

As mentioned previously, the field force on the vehicle is determined by the field strength vector, road conditions at the vehicle's location, the vehicle's attributes, and driver's behavior characteristics. Here, we define the specific form of (8) as

$$\boldsymbol{F}_{ij} = \boldsymbol{F}(\boldsymbol{E}_{ij}, M_j, R_j, DR_j) = \boldsymbol{E}_{ij} \cdot M_j \cdot R_j \cdot (1 + DR_j) \tag{22}$$

3.3. Indicators of driving safety

According to (7), (10), (18), (21), and (22), we obtain the safety potential energy of vehicle j under three types of driving risks

$$\begin{cases} \mathrm{SPE}_{R,aj} = \frac{KR_aR_jM_aM_j}{(k_1-1)|\boldsymbol{r}_{aj}|^{k_1-1}} \\ \mathrm{SPE}_{V,bj} = \frac{KR_bR_jM_bM_jk_3}{(k_1-1)|\boldsymbol{r}_{bj}|^{k_1-1}} \cdot \left[\frac{(k_3-|\boldsymbol{v}_b|\cos\theta_b)^{1-k_1}}{k_3-|\boldsymbol{v}_b|}\right]^{\frac{1}{k_1}} \\ \mathrm{SPE}_{D,cj} = DR_c \cdot SE_{V,cj} \end{cases} \tag{23}$$

Specifically, according to (19), the safety potential energy of vehicle j in the potential field formed by the lane marker a is

$$\mathrm{SPE}_{R,aj,L} = \frac{LT_aR_aR_jM_j(1+DR_j)}{k_2+1} \cdot \left(\frac{D}{2} - |\boldsymbol{r}_{aj}|\right)^{k_2+1} \tag{24}$$

Moreover, according to (11) and (22), we can obtain the temporal change rate of safety potential energy

$$\dot{\mathrm{SPE}}_{ij} = M_jR_j(1+DR_j)\boldsymbol{E}_{ij} \cdot (\boldsymbol{v}_j - \boldsymbol{v}_i) \tag{25}$$

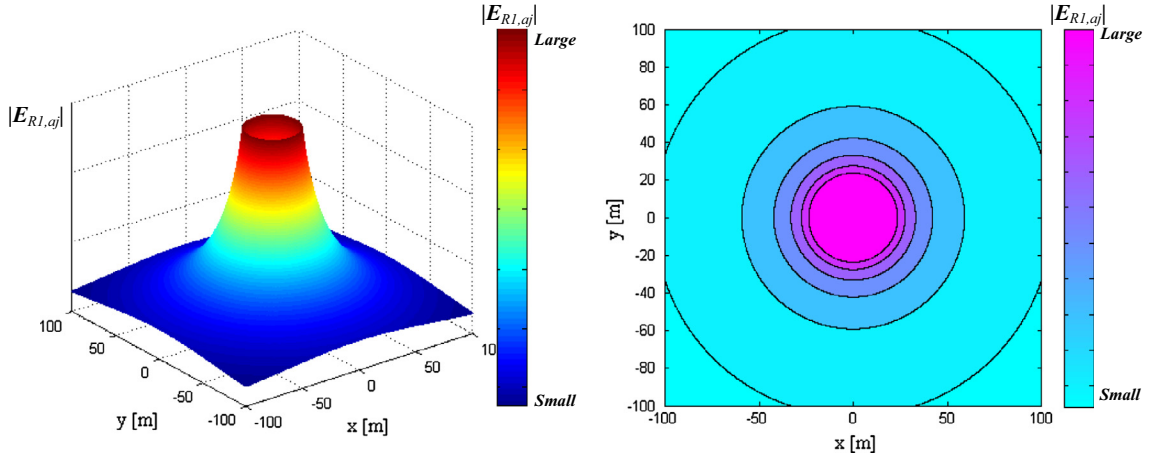

Fig. 4. Sketches of the potential field strength given by (18) (set $K = 0.5, R_a = 1, k_1 = 1.2$).

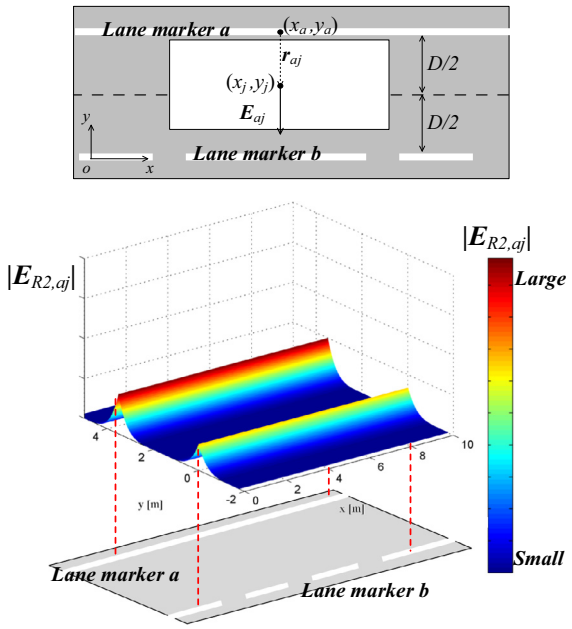

Fig. 5. Sketches of the potential field strength given by (19) (set $LT_{a1} = 3, LT_{a2} = 2, R_a = 1, k_2 = 1.2$).

Afterwards, to obtain the total safety potential energy, the weights of individual safety potential energies should be defined. According to (12), h_i (the weight of SPE_{ij}) is defined as

$$h_i = h(d_i, D) = \min\left\{\left(\frac{D}{2d_i}\right)^{k_4}, 1\right\} \tag{26}$$

where k_4 (>0) is a undetermined constant.

Finally, we define the specific form of the driving safety index as

$$\mathrm{DSI}_j = \mathrm{DSI}(\mathrm{SPE}_j, \dot{\mathrm{SPE}}_j) = \alpha \cdot \mathrm{SPE}_j + (1-\alpha) \cdot \dot{\mathrm{SPE}}_j \tag{27}$$

where α is weight, which is set to ensure balance between the spatial driving risk and the temporal driving risk.

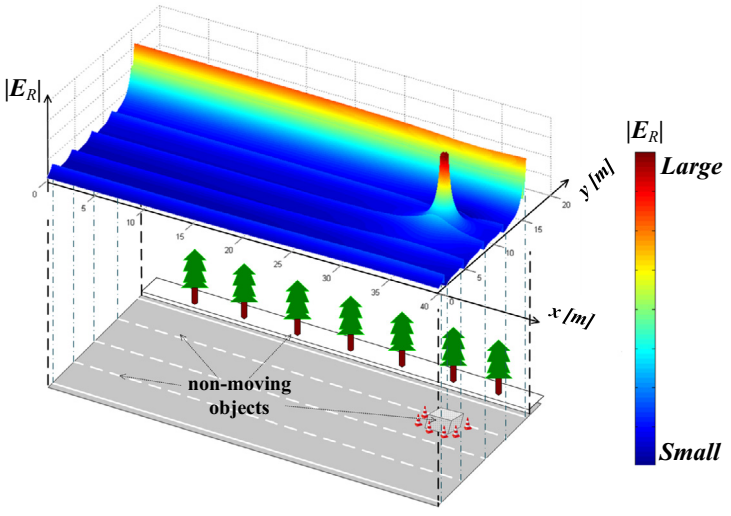

Fig. 6. Nonmoving objects and the field strength of their corresponding potential field (set $LT_{a1} = 3, LT_{a2} = 2, R_a = 1, k_1 = 1, k_2 = 1.2, k_3 = 45, R = 1, T = 1, K = 0.5, DR = 0.5$).

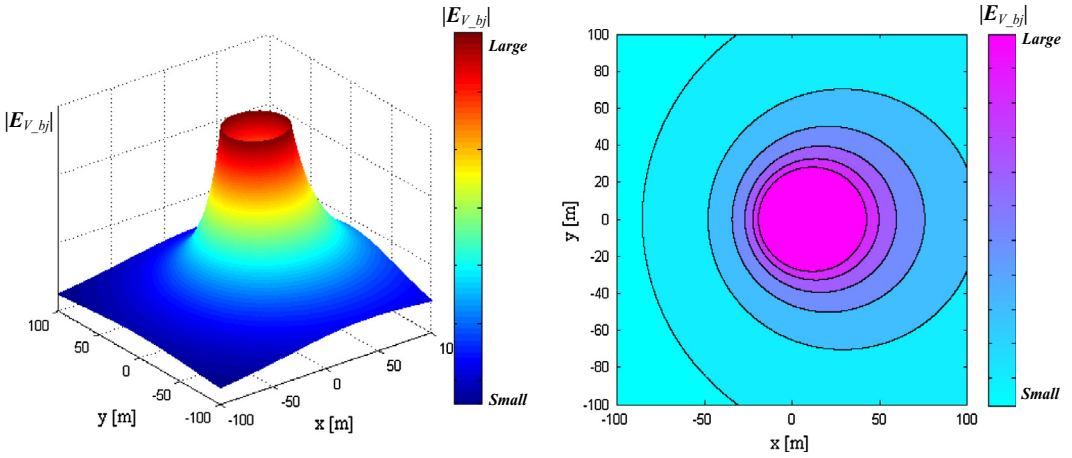

Fig. 7. Sketches of the potential field strength given by (21) (set $K = 0.5, R_a = 1, k_1 = 1.2, k_3 = 45$).

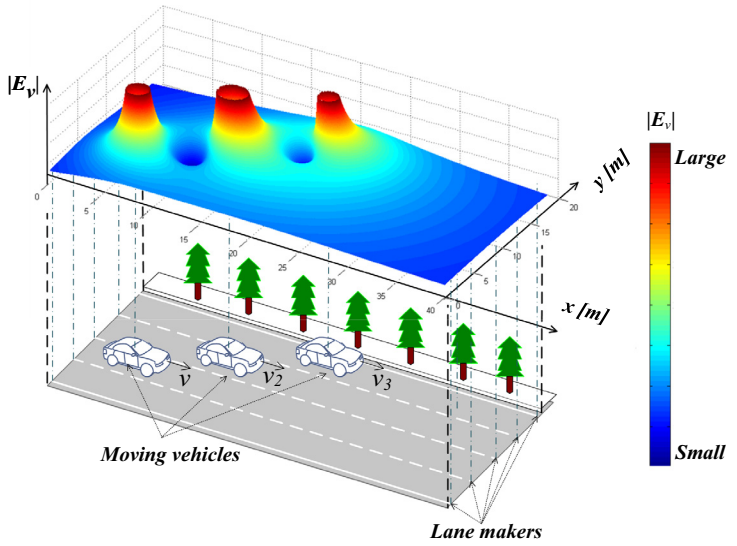

Fig. 8. Moving objects and the field strength of their corresponding safety field (set $LT_{a1} = 0, LT_{a2} = 0, R_a = 1, k_1 = 1, k_2 = 1.2, k_3 = 45, R = 1, T = 1, K = 0.5, DR = 0.5$).

4. Collision warning algorithm based on driving safety field model

4.1. Model application in typical multi-vehicle scenario

A typical multi-vehicle scenario is shown in Fig. 10, where three vehicles (vehicle 1: ego vehicle, vehicle 2: leading vehicle, vehicle 3: adjacent vehicle) are driving along the center of their lanes. $\boldsymbol{v}_1$, $\boldsymbol{v}_2$, and $\boldsymbol{v}_3$ are velocity vectors of vehicle 1, vehicle 2, and vehicle 3, respectively.

Driving safety of vehicle 1 is influenced by the current lane markers, vehicle 2, and vehicle 3. Meanwhile, considering that vehicle 1 is driving along the centerline of its lane, where the field strength vectors of the driving safety field formed by the lane markers are both zero, only vehicle 2 and vehicle 3 need to be considered. The influence of vehicle 2 and vehicle 3 on the driving safety of vehicle 1 can be denoted as a driving safety field consisting of two parts: (i) the kinetic fields formed by vehicles 2 and 3, and (ii) behavior fields formed by the drivers of vehicles 2 and 3. The field strength vectors of the above two fields point from vehicle 2 and vehicle 3 toward vehicle 1. Moreover, according to the specific model given in above section, we obtain

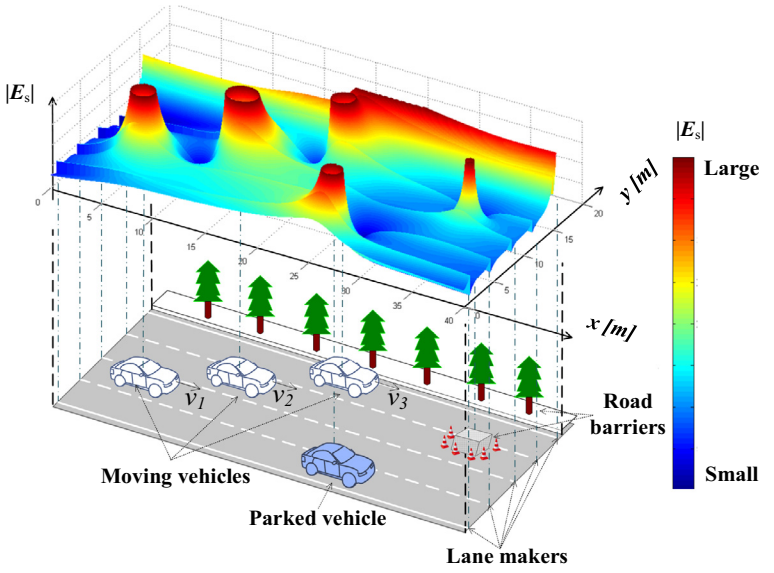

Fig. 9. Multi-vehicle scenario and the field strength of their corresponding driving safety field (set $LT_{a1} = 3, LT_{a2} = 2, R_a = 1, k_1 = 1, k_2 = 1.2, k_3 = 45, R = 1, T = 1, K = 0.5, DR = 0.5$).

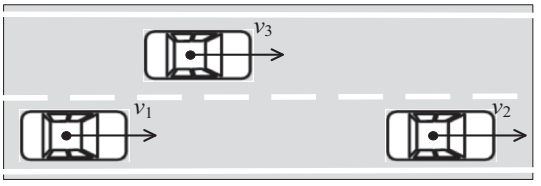

Fig. 10. Typical scenario involving multiple vehicles.

$$
\begin{cases}
\boldsymbol{E}_{V,i1} = \frac{K \cdot R_i \cdot M_i \cdot k_3}{(k_3 - |\boldsymbol{v}_i| cos\theta_i) \cdot |\boldsymbol{r}_{i1}|^{k_1}} \cdot \frac{-\nabla \boldsymbol{E}_{V,i1}}{|\nabla \boldsymbol{E}_{V,i1}|} \\
\boldsymbol{E}_{D,i1} = DR_i \cdot \boldsymbol{E}_{V,i1} \\
\boldsymbol{E}_{i1} = \boldsymbol{E}_{V,i1} + \boldsymbol{E}_{D,i1} \\
\mathrm{SPE}_{V,i1} = \frac{KR_iR_1M_iM_1(1+DR_i)k_3}{(k_1-1)|\boldsymbol{r}_{21}|^{k_1-1}} \cdot \left[\frac{(k_3 - |\boldsymbol{v}_i|\cos\theta_i)^{1-k_1}}{k_3 - |\boldsymbol{v}_i|}\right]^{\frac{1}{k_1}} \\
\mathrm{SPE}_{D,i1} = DR_i \cdot SE_{V_{i1}} \\
h_i = \min\left\{\left(\frac{D}{2d_i}\right)^{k_4}, 1\right\} \\
\mathrm{SPE}_1 = \sum_{i=2}^{3}[h_i \cdot (\mathrm{SPE}_{V,i1} + \mathrm{SPE}_{D,i1})] \\
\dot{\mathrm{SPE}}_{i1} = M_1R_1(1 + DR_1)\boldsymbol{E}_{i1} \cdot (\boldsymbol{v}_i - \boldsymbol{v}_1) \\
\dot{\mathrm{SPE}}_1 = \sum_{i=2}^{3}(h_i \cdot \dot{\mathrm{SPE}}_{i1}) \\
\mathrm{DSI}_1 = \alpha \cdot SPE_1 + (1-\alpha) \cdot \dot{\mathrm{SPE}}_1
\end{cases}
\tag{28}
$$

where $\boldsymbol{E}_{V,i1}$ and $\boldsymbol{E}_{D,i1}$ are the field strength vectors acting on vehicle 1 in the kinetic field and behavior field formed by vehicle i, respectively. $\boldsymbol{E}_{i1}$ is the total field strength vector acting on vehicle 1 in the driving risk field formed by vehicle i. $\mathrm{SPE}_{V,i1}$ and $\mathrm{SPE}_{D,i1}$ are the safety potential energies that vehicle 1 has in the kinetic field and behavior field formed by vehicle i, respectively. SPE_1 is the total safety potential energy. DSI_1 is the driving safety index of vehicle 1, which represents the driving risk that vehicle 1 faces. h_i is the weighting factor of vehicle i, M_i is the virtual mass of vehicle i, and R_i is the influencing factor pertaining to road condition at the location of vehicle i. $\boldsymbol{r}_{i1}$ is distance vector between vehicle 1 and vehicle i, d_i is the distance between the mass center of vehicle i and the centerline of the right lane, and θ_i is the angle between the directions of $\boldsymbol{v}_i$ and $\boldsymbol{r}_{i1}\,(i = 2, 3)$. After simplifying (28), we obtain

$$\begin{cases} \mathrm{SPE}_1 = KM_1R_1(1+DR_1)\cdot\sum_{i=2}^{3}\left\{\frac{h_iR_iM_i(1+DR_i)k_3}{(k_1-1)|\boldsymbol{r}_{21}|^{k_1-1}}\cdot\left[\frac{(k_3-|\boldsymbol{v}_i|\cos\theta_i)^{1-k_1}}{k_3-|\boldsymbol{v}_i|}\right]^{\frac{1}{k_1}}\right\} \\ \dot{\mathrm{SPE}}_1 = KM_1R_1(1+DR_1)\cdot\sum_{i=2}^{3}\frac{h_iR_iM_i(1+DR_i)k_3\nabla\boldsymbol{E}_{V,i1}\cdot(\boldsymbol{v}_1-\boldsymbol{v}_i)}{(k_3-|\boldsymbol{v}_i|\cos\theta_i)\cdot|\boldsymbol{r}_{i1}|^{k_1}\cdot|\nabla\boldsymbol{E}_{V,i1}|} \\ \mathrm{DSI}_1 = \alpha\cdot\mathrm{SPE}_1+(1-\alpha)\cdot\dot{\mathrm{SPE}}_1 \end{cases} \tag{29}$$

4.2. Relative driving safety index

The driving safety index of vehicle 1 (DSI_1) can denote the driving risk vehicle 1 faces. However, DSI_1 is an absolute risk index and its variation range is uncertain. Therefore, when using DSI_1 to evaluate the driving risk directly, it is difficult to determine the threshold of warning level of the collision warning algorithm. To solve this problem, a new index called the relative driving safety index (RDSI) is proposed. And the relative driving risk index of vehicle 1 (RDSI_1) is defined as

$$\mathrm{RDSI}_1 = \frac{\mathrm{DSI}_1}{\mathrm{DSI}^*} \tag{30}$$

where DSI^* is the standard driving safety index of vehicle 1 in a specific scenario. As mentioned previously, TTC and THW have been widely regarded to measure the potential driving risk in a car following scenario. Moreover the 1 s THW and 4 s TTC criterion is a suggested warning criterion (Janssen and Nilsson, 1992). Therefore, a typical dangerous scenario is set as the specific scenario. In the scenario, vehicle 1 is following another vehicle (the same type, physical mass, road condition influencing factor and driver risk factor with vehicle 1) with the 1 s THW and 4 s TTC. These two vehicles are both driving along the centerline of their lane. Moreover, there are no other vehicles around. Different from DSI_1, RDSI_1 has a relatively stable value range (see Fig. 11).

4.3. Collision warning algorithm based on driving safety field model

The collision warning algorithm of this system is designed based on the relative driving safety index (RDSI) and a three-level (safe, dangerous, and very dangerous) warning effort is adopted.

(1) Warning Level I: safe

$$IF\ \ \mathrm{RDSI} < W_1,\ THEN\ C_W = 0.$$

W_1 is the threshold of the safety driving state, C_W is the warning level signal: $C_W = 0$ means no warning, safety; $C_W = 1$ means dangerous with a discontinuous buzzing for warning; and $C_W = 2$ means very dangerous with a steady buzzing for warning.

(2) Warning Level II: dangerous

$$IF\ W_1 < \mathrm{RDSI} < W_2,\ THEN\ C_W = 1.$$

W_2 is the threshold of the dangerous driving state. When RDSI is larger than the threshold of the safety driving state, smaller than that of the dangerous driving state, the warning level is dangerous. The system sends a discontinuous buzzing for warning.

(3) Warning Level III: very dangerous

$$IF\ \mathrm{RDSI} > W_2,\ THEN\ C_W = 2.$$

When RDSI is larger than the threshold of the dangerous driving state, the warning level is very dangerous and the system sends a discontinuous buzzing for warning.

5. Field experiments and analysis of results

5.1. Field experiments

Experiments using real vehicles were conducted to verify the warning algorithm. Twenty-four drivers (twenty male, four female) were invited, with each driving on a straight urban four-lane road in Beijing (lane width = 3.75 m). The length of the experimental route was about 6 km. The experiment scenario is shown in Fig. 12.

The experiments were conducted using three experimental vehicles, which are shown in Fig. 13(a). Each vehicle was equipped with a GPS and an on-board computer to collect and record GPS position and time readings, which were used for data synchronization. An oil pressure sensor and two acceleration sensors were attached to each vehicle to measure the brake pressure and longitudinal and lateral acceleration, and all signals were sent to the CAN bus. The velocity, accelerator pedal position, and brake pedal on/off signal were also collected from the CAN bus. During the experiments, the signals

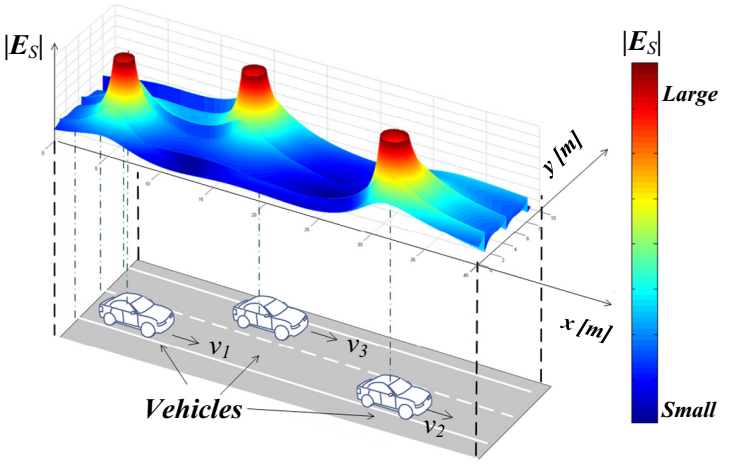

Fig. 11. Typical multi-vehicle scenario and the field strength of their corresponding safety field (set $LT_{a1} = 3, LT_{a2} = 2, R_a = 1, k_1 = 1, k_2 = 1.2, k_3 = 45$, $R = 1, T = 1, K = 0.5, DR = 0.5$).

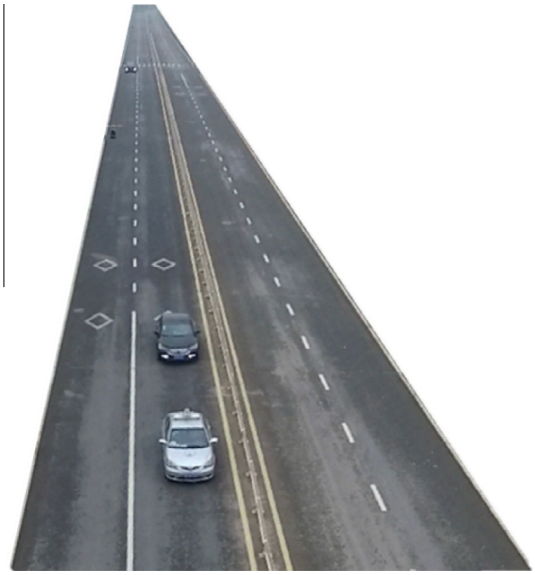

Fig. 12. Real scenario.

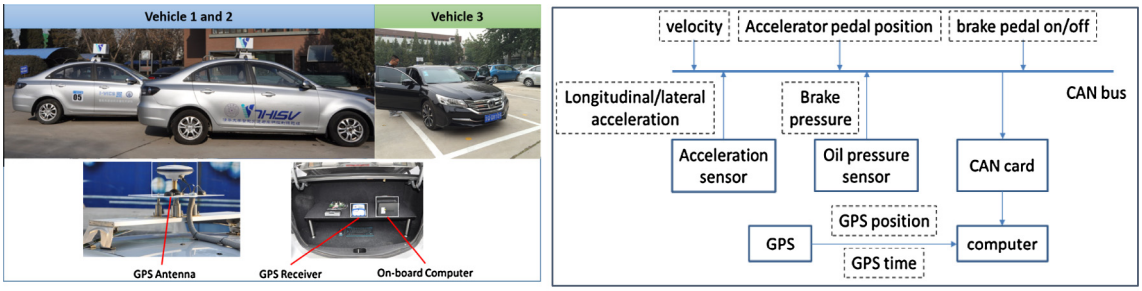

(a) (b)

Fig. 13. Experimental vehicles and Information flow.

from the CAN bus were transmitted to the computer through a CAN card and recorded along with GPS information in a text file. The data collection frequency was 5 Hz. The information flow is shown in Fig. 13(b).

The experiment route was the ShuiNan road, ChangPing district, northwest of Beijing. The experiments were conducted under scenarios: a car-following scenario and a cut-in scenario (see Figs. 14 through 19).

(1) Car-following scenario

The subject drivers were asked to drive vehicle 1 following vehicle 2 with no other vehicles nearby. The speed of vehicle 2 was automatically controlled according to the equation $v_2 = 45 + 20\sin(2\pi t/T)$ km/h. Moreover the period T (s), which ranges between $[24, 48]$, changes after every period. T series were set as $\{(24, 36), (30, 30), (32, 28), (25, 35), (34, 26), (27, 33)\}$, which means the experiment of this scenario lasted 6 min in total for each driver. The longitudinal speed, acceleration, GPS, brake signal and pressure of vehicles 1 and 2 were recorded during the experiment.

(2) Cut-in scenario

The subject drivers were asked to drive vehicle 1 following vehicle 2 with vehicle 3 running in the adjacent lane. Vehicle 2 moved in the same way as in the car-following scenario. Vehicle 3 drove in the adjacent lane, and kept itself between vehicles 1 and 2 longitudinally.

In addition, during the experiment vehicle 3 was controlled to satisfied the following requirements: (i) running straight in adjacent lane in most of test time; (ii) 4 times cut-in motion if a sizable gap were available during the experiment; and (iii) 9 times swing motion (shifted to the right lane as if a cut-in would happen but moved back quickly).

5.2. Comparison of RDSI and TTCi

TTCi (or TTC) is widely used in forward collision warning system, such as Kiefer's CAMP method and improved safety indicator based on TTC (Kiefer et al., 1999, 2005, 2006). In Kiefer's research, a subject vehicle and a principle other vehicle were used to research the examined drivers last-second braking and steering (or lane-change) judgments under a wide range of vehicle-to-vehicle kinematic conditions decelerating and stationary trials. In this paper, the real vehicle experiment, we considered both car-following scenario and adjacent vehicle cut-in scenario, after the real vehicle experiment, we researched both value of TTCi and RDSI. Our RDSI showed a high value when the brake pedal is pushed by the driver, the value of TTCi also showed a rise tendency, but the changes are not very noticeable.

In addition, for this algorithm, we designed a real vehicle experiment to illuminate it. The value of RDSI represents the risk state of vehicle. First, the surround traffic information was collected by using sensor and communication technologies, then, RDSI could be evaluated by using Eqs. (23)–(30). This index is quite different with TTC or TTCi, but to a certain extent, there are certain things in common between them.

During the real vehicles experiment, we got 300 min of valid data, including 150 min of car-following data in experiment A, 100 min of vehicle 3 straight driving data and 50 min of vehicle 3 for 99 cut-in activities and 199 attempts to cut-in.

24 test drivers were invited to attend this experiment. We collected the data of vehicle state, and this histogram showed the TTCi frequency distribution of 1 s before braking and 1 s after braking.

A total of TTCi data during 1 s before braking (namely $\mathrm{TTCi}^{\mathrm{B}}$) included 1608 frames, every time we collected the data of 1 s before braking for 6 frames, so the total time of the $\mathrm{TTCi}^{\mathrm{B}}$ data was 268 s, and the mean value was 0.0912 s^{-1}. Similarly, a total of TTCi data during 1 s after braking (namely $\mathrm{TTCi}^{\mathrm{A}}$) included 1596 frames, the total time of the $\mathrm{TTCi}^{\mathrm{A}}$ data was 266 s, and the mean value was 0.0229 s^{-1}. In this paper, we used the method of nonparametric test to measure the difference of distribution between $\mathrm{TTCi}^{\mathrm{A}}$ and $\mathrm{TTCi}^{\mathrm{B}}$, because both of them were not close to the normal distribution.

In order to receive an accurate test result, both Kolmogorov-Smirnov Z method and Mann-Whitney U methods were used, and both results shown the significant difference under the confidence level of 0.1%, that is to say, $\mathrm{TTCi}^{\mathrm{B}}$ was greater than $\mathrm{TTCi}^{\mathrm{A}}$ obviously. The result means the brake pedal was pushed by test driver in vehicle 1 when the value of TTCi in a high level, and loosen the brake pedal when the TTCi declined to a certain value. Therefore, TTCi could evaluate the driving risk of vehicle 1 in the first experiment, and the large value of TTCi means a larger driving risk.

This histogram showed the RDSI_1 frequency distribution of 1 s before braking and 1 s after braking. Similar to the above data, a total of RDSI_1 data during 1 s before braking (namely $\mathrm{RDSI}_1^{\mathrm{B}}$) included 1608 frames, the total time of the $\mathrm{RDSI}_1^{\mathrm{B}}$ data was 268 s, and the mean value was 0.0912 s^{-1}. Similarly, a total of $\mathrm{RDSI}_1^{\mathrm{B}}$ data during 1 s after braking (namely $\mathrm{RDSI}_1^{\mathrm{A}}$) included 1596 frames, the total time of the $\mathrm{RDSI}_1^{\mathrm{A}}$ data was 266 s, and the mean value was 0.0229 s^{-1}. We used the same method to measure the difference of distribution between $\mathrm{RDSI}_1^{\mathrm{A}}$ and $\mathrm{RDSI}_1^{\mathrm{B}}$ in this part, and we also found that the significant difference under the confidence level of 0.1%, that is to say, RDSI_1 could also evaluate the driving risk of vehicle 1 in the first experiment, and the large value of RDSI_1 means a larger driving risk.

Those 24 test drivers were invited to attend the experiment B after they finished the first experiment. This time, we also analyzed the TTCi frequency distribution of 1 s before braking and 1 s after braking.

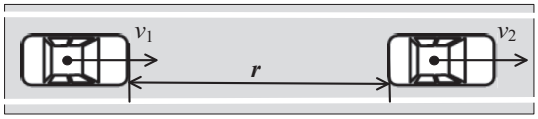

Fig. 14. Car-following scenario.

The data of the 24 test drivers were collected in the experiment B. Similar to the experiment A, a total of TTCi data during 1 s before braking (namely $TTCi^B$) included 1554 frames, the total time of the $TTCi^B$ data was 259 s, and the mean value was 0.0842 s^{-1}. Similarly, a total of TTCi data during 1 s after braking (namely $TTCi^A$) included 1536 frames, the total time of the $TTCi^A$ data was 256 s, and the mean value was −0.0389 s^{-1}. We used the same method to measure the difference of distribution between $TTCi^A$ and $TTCi^B$ in experiment B, and we also found that the significant difference under the confidence level of 0.1%.

But the data of $TTCi^B$ which value is less than zero accounts for 5.53% of the total, this percentage is much different from the experiment A (0.37%). The above research mentioned a negative value of TTCi means the vehicle ahead was driving away, this means safe. But the data of 5.53% means may be some scenarios in danger and therefore it cannot show the driving risk correctly.

Similar to the above research, we compared the $RDSI_1$ frequency distribution in 2 s including 1 s before braking and another 1 s after braking.

In experiment B, a total of $RDSI_1$ data during 1 s before braking (namely $RDSI_1^B$) included 1554 frames, the total time of the $RDSI_1^B$ data was 259 s, and the mean value was 0.575 s^{-1}. Similarly, a total of $RDSI_1$ data during 1 s after braking (namely $RDSI_1^A$) included 1536 frames, the total time of the $RDSI_1^A$ data was 256 s, and the mean value was 0.268 s^{-1}. We used the same method to measure the difference of distribution between $RDSI_1^A$ and $RDSI_1^B$ in experiment B, in contrast, we found that the significant difference under the confidence level of 0.1%. Therefore, we can use $RDSI_1$ to evaluate the driving risk.

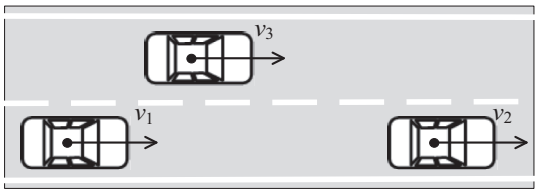

Fig. 15. Cut-in scenario.

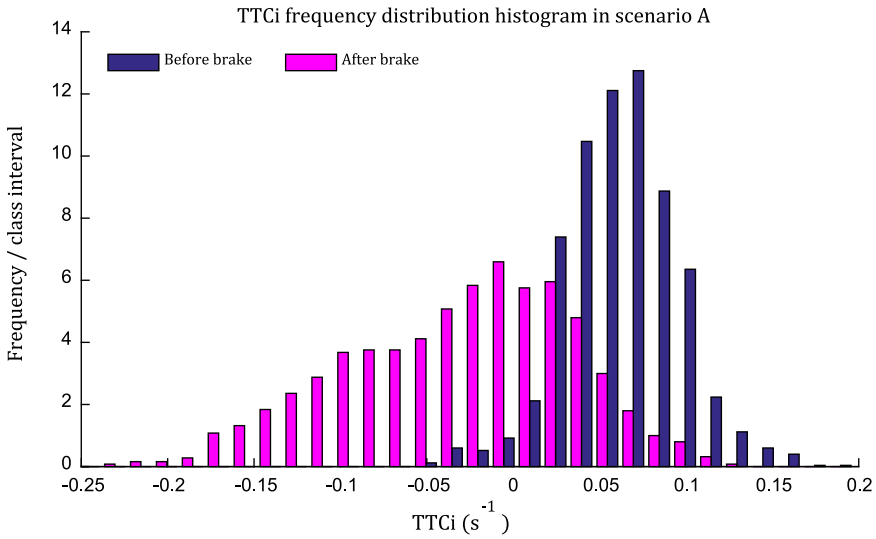

Fig. 16. The TTCi frequency distribution during the brake activity in experiment A.

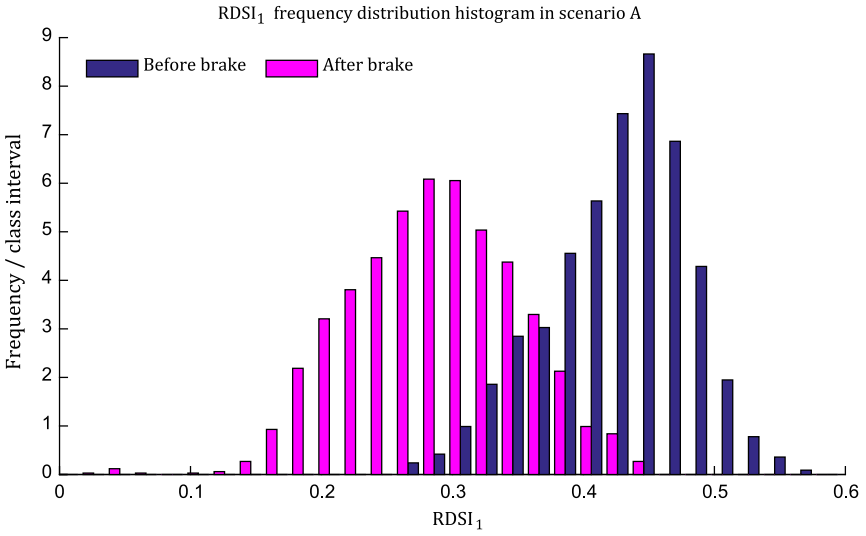

Fig. 17. The $RDSI_1$ frequency distribution during the brake activity in experiment A.

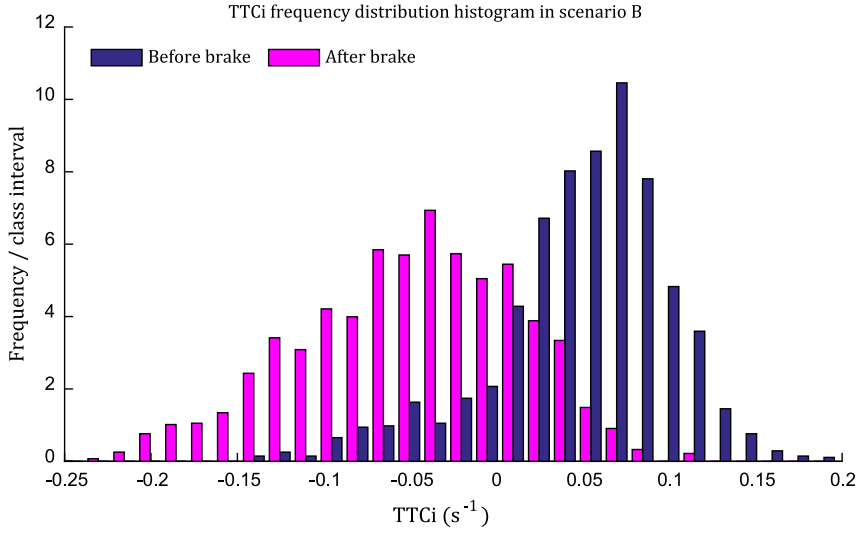

Fig. 18. The TTCi frequency distribution during the brake activity in experiment B.

5.3. Analysis of results

The three experimental vehicles were the same type of cars, in this case $T_1 = T_2 = T_3$. Owing to the similar road conditions of the lanes, the values of R_1, R_2, and R_3 were equal. Moreover, the driver risk factors were assumed to be the same. Hence, to simplify the calculation, we chose the following set of parameters: $K = 0.5$, $R_1 = R_2 = R_3 = 1$, $T_1 = T_2 = T_3 = 1$, $DR_1 = DR_2 = DR_3 = 0.5$, $k_1 = 1$, $k_3 = 45$, $k_4 = 1$, $m_1 = m_2 = m_3 = 1400$ kg, $\alpha = 0.06$.

Thereafter, according to Eqs. (29) and (30), the relative driving safety index of vehicle 1 ($RDSI_1$) is calculated in real time. When $RDSI_1$ reaches the threshold, the driver assistance system prompts the driver and then s/he starts to decelerate (by releasing the accelerators pedal or braking) to avoid potential risk. We defined the threshold W_1 and W_2 at 50th and 90th percentiles of RDSI data respectively.

During this experiment, we attained a series of data for three vehicles, including 98 cut-in activities and 199 attempts to cut-in. Some typical results are shown in Fig. 20. According to Fig. 20(a), the $RDSI_1$ curve agrees with the TTCi curve ($TTCi = (v_1 - v_2)/|\mathbf{r}_{21}|$), which means that in the experimental scenario, $RDSI_1$ can represent the driving potential risk because TTCi is admitted as an evaluation of potential risk. More interestingly, in Fig. 20(b), we observe that the driver begins braking with a rather small TTCi value, which in this case is actually −0.005/s. This small value of TTCi represents "safe."

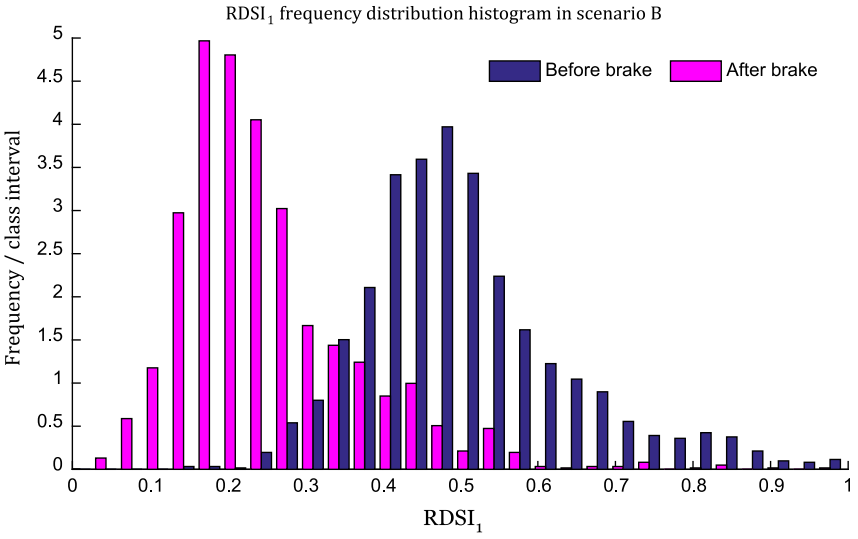

Fig. 19. The $RDSI_1$ frequency distribution during the brake activity in experiment B.

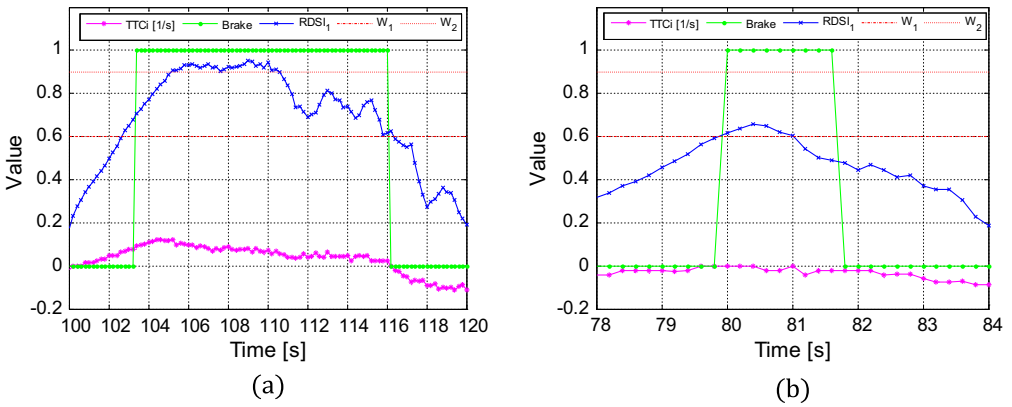

Fig. 20. Experimental results.

However, the driver applies brake, which implies that s/he thinks the driving state at that moment might be dangerous. The reason is that at that moment, the possibility of vehicle 3 cutting in is relatively large. Hence, the driver brakes even though vehicle 1 is far away. TTCi cannot show the influence of vehicle 3, and it is not reliable when the influence of vehicle 3 is relatively large, especially at the moment at which vehicle 3 may cut in. In contrast, the $RDSI_1$ curve maintains similar reliability to help evaluate the driving risk compared with the curve in Fig. 20(a), which is because of the calculation of $RDSI_1$ that has already contained the consideration of vehicle 3. In addition, this shows the advantages of the driving safety field model in evaluating driving risk in multi-vehicle scenarios.

6. Discussion

The present study found the unified driving safety field theory with merged the parameters of drivers, vehicles, and environment. This suggested that driving safety field can capture the state of driving risk in the traffic environment. This study aim to establish the frame of a warning algorithm. Every factor in real traffic environment can be expressed by using the algorithm, moreover it would benefit for detect the traffic risk and path planning. In physics, a field is a physical quantity that has a value for each point in space and time (McMullin, 2002). In real traffic environment, in order to make the risk more intuitive, the traffic risk is described by assigning a vector to each point on a map by using this method. Each vector represents the state of the risk at that point, thereby revealing the potential of this method in driving-safety research more generally.

In this paper, we put in a great deal of effort on establishing the general model, the specific model and the collision algorithm, compare to our presented study, the frame of the algorithm has become clearer. However, there are a few problems remaining to be solved.

(1) Driver behavior

Driver behavior is very complex, which is influenced by many factors, such as limited perception, response delay, distraction, inattention, haste, and fatigue. However, it's not practical to consider all these factors in this paper. Therefore, we just build a framework here to consider driver factors, and classified all these factors into four aspects, namely, physical-psychological, cognition, driving skill, and traffic violations. In addition, we will continue implementing following researches in this area.

(2) Parameter choice and calibration

This algorithm considered a number of parameters, such as the visibility, adhesion coefficient, road curvature, and the slope of the road or the risk factors of driver's physical-psychological, cognition, driving skill, and traffic violations, moreover, this algorithm contains a few of dimensionless parameters. Every parameter has its own meaning. In this research, we did not calibrated these parameters, more experiments should be conducted before we can come to a conclusion. We take much more factors into account so that the algorithm can reflect real performance of the complicated traffic environment. The modified algorithm is also effective under the present condition.

However, the parameters which are decided by traffic environment could be obtained by fitting traffic accident statistic data. At present there had a lot of related research on traffic accidents data analysis. Kloeden et al. (2002) found a quantitative relation between the traffic risk with urban roads speed limit. Cameron and Elvik (2010) proved the availability of Nilsson's Power Model by traffic accident statistic data analysis. Elvik (2013) presented a re-analysis of the Power Model of the relationship between the mean speed of traffic and road safety. Ruikar (2013) studied Indian traffic accident casualties by the traffic accident statistic data. The parameters of driver behavior could be obtained by detecting and analyzing human body physiology signal, because when a human in danger or his mood changes, the signal of electrocardiogram, electrodermal activity and electroencephalogram will change accordingly (Holper et al., 2014; Dupuy et al., 2014; van Tricht et al., 2014). Above all, it is certainly possible that the parameters for the driving safety field model will be calibrated in the future.

(3) Further explore of the theoretical structure

In present research of this paper, the vehicle dynamics has not yet been considered, because there are so many unknown parameters need to ascertain in driving safety field theory, so, in the early stages of the formation of this theory, we should simplify the frame of the model, but we will improve the model structure continuously by consider the acceleration/deceleration, lateral velocity of both ego vehicle and adjacent vehicles, and we also could consider the different driving conditions such as the three stages of a rollover accident, including Pre-trip phase, Trip phase, and Post-trip phase. It could be discussed in more details in future research and development.

(4) The improvement of the experimental verification method

In Section 5 it was shown, our experiment divided into two scenarios, one is following scenario, the other is cut-in scenario, Scenario options of this real vehicle experiment has some limitation. Further research is needed for a driving simulator experiment, which can simulate the effects of the warning algorithm in different kinds of scenario, and we can use real vehicle experiment to test and verify.

7. Conclusion

In this study, we have summarized the previous article (Wang et al., 2014), based on which a modified general model and, further, specific model of driving safety field were proposed. This modified model of the driving safety field is described briefly, which can be applied to cases that are more general in nature and, meanwhile, can be tailored to suit a modeler's particular situation. The specific model reflected a concrete scenario of driving, and the graphs given by those equations, to a certain extent, could provide a visual verification of the model. Based on the specific model, a vehicle collision warning algorithm was developed.

The proposed driving safety warning algorithm is able to incorporate multi-vehicle driving scenarios. Compared with existing vehicle-collision-warning algorithms, this algorithm includes a greater number of traffic factors and is not limited to simplified scenarios such as car following and lane changing. Moreover, field experiments were conducted to verify the proposed algorithm. According to the analysis of the experimental results, in both scenarios, the algorithm is able to represent the risk of the collision efficiently and warn the driver in real time. In particular, compared with TTCi, the algorithm shows better efficiency in multi-vehicle scenarios, which, to a large extent, indicates that the proposed algorithm can be applied to multi-vehicle driving scenarios.

However, our framework contained several factors of driver, vehicle and road, which make it difficult to be applied. Although that we try to reflect the truth by incorporating as much details as possible, we have to strike a balance between model fidelity and usability. Therefore, rather than including everything, we may have to capture some major factors in a simplified way during research. Even though, the model has posed some challenges on model calibration and validation. For-

tunately, with limited field data collection, especially with the help of connected vehicle technology and complemented by human factors studies as well as published results in similar areas, the task should be accomplishable. Nevertheless, it is fair to state that, in modeling, truth comes with costs.

Future work will focus on two major aspects: one for further study of methods to determine the parameters of the model, and the other for applications. Moreover the applications will focus on the intelligent control of the vehicle to avoid traffic risk and make safety assessments for the accident-prone road sections based on the driving safety field model.

Acknowledgment

This work was supported by the National Natural Science Foundation of China, No. 51475254. We appreciate Mr. Hongmao Qin for his valuable comments and helpful work. We would also like to thank Mr. ManJiang Hu, Xiang Gao, Biao Xu, XiaoHui Qin, and Ms. Yue Liu for their help in field experiments.

References

Abdel-Aty, M., Cunningham, R., Gayah, V., Hsia, L., 2006. Dynamic variable speed limit strategies for real-time crash risk reduction on freeways. Transp. Res. Rec.: J. Transp. Res. Board 38, 108–116.

Beard, R.W., Kingston, D., Quigley, M., Snyder, D., Christiansen, R., Johnson, W., McLain, T., Goodrich, M., 2005. Autonomous vehicle technologies for small fixed-wing UAVs. J. Aerosp. Comput. Inform. Commun. 2 (1), 92–108.

Bourhis, G., Horn, O., Habert, O., Pruski, A., 2001. An autonomous vehicle for people with motor disabilities. IEEE Robot. Autom. Mag. 8 (1), 20–28.

Caliendo, C., Maurizio, G., Alessandra, P., 2007. A crash-prediction model for multilane roads. Accid. Anal. Prev. 39, 657–670.

Cameron, M.H., Elvik, R., 2010. Nilsson's power model connecting speed and road trauma: applicability by road type and alternative models for urban roads. Accid. Anal. Prev. 42, 1908–1915.

Cui, Y., Ge, S.S., 2003. Autonomous vehicle positioning with GPS in urban canyon environments. IEEE Trans. Robot. Autom. 19 (1), 15–25.

Dabbour, Essam, Easa, Said, 2014. Proposed collision warning system for right-turning vehicles at two-way stop-controlled rural intersections. Transp. Res. Part C 42, 121–131.

Dupuy, F.E., Clarke, A.R., Barry, R.J., Selikowitz, M., McCarthy, R., 2014. EEG and electrodermal activity in girls with attention-deficit/hyperactivity disorder. Clin. Neurophysiol. 125 (3), 491–499.

Elvik, R., 2013. A re-parameterisation of the power model of the relationship between the speed of traffic and the number of accidents and accident victims. Accid. Anal. Prev. 50, 854–860.

Heddebaut, M., Rioult, J., Ghys, J.P., Gransart, C., Ambellouis, S., 2005. Broadband vehicle-to-vehicle communication using an extended autonomous cruise control sensor. Meas. Sci. Technol. 16, 1363–1373.

Holper, L., Wolf, M., Tobler, P.N., 2014. Comparison of functional near-infrared spectroscopy and electrodermal activity in assessing objective versus subjective risk during risky financial decisions. NeuroImage 84, 833–842.

Jacob, Celine, Abdulhai, Baher, 2010. Machine learning for multi-jurisdictional optimal traffic corridor control original. Transp. Res. Part A: Policy Pract. 44 (2), 53–64.

Janssen, W.J., Nilsson, L., 1992. An Experimental Evaluation of In-vehicle Collision Avoidance Systems. VTI Sartryck; nr. 181.

Jian, Xiao-Xia, Wong, S.C., Zhang, Peng, Choi, Keechoo, Li, Hong, Zhang, Xiaoning, 2014. Perceived cost potential field cellular automata model with an aggregated force field for pedestrian dynamics. Transp. Res. Part C 42, 200–210.

Khatib, O., 1986. Real-time obstacle avoidance for manipulators and mobile robots. Int. J. Rob. Res. 5 (1), 90–98.

Kiefer, R., LeBlanc, D., Palmer, M., Salinger, J., Deering, Z.R., Shulman, M., 1999. Development and Validation of Functional Definitions and Evaluation Procedures for Collision Warning/Avoidance Systems, Technical Report. DOT HS 808 964, National Highway Traffic Safety Administration, U.S. Department of Transportation, August 1999, Final Report.

Kiefer, R.J. et al, 2005. Developing an inverse time-to-collision crash alert timing approach based on drivers' last-second braking and steering judgments. Accid. Anal. Prev. 37 (2), 295–303.

Kiefer, R.J., Flannagan, C.A., Christian, J., 2006. Time-to-collision judgments under realistic driving conditions. Hum. Fact.: J. Hum. Fact. Ergon. Soc. 48, 334–345.

Kitamura, Y., Tanaka, T., Kishino, F., et al., 1995. 3-D path planning in a dynamic environment using an octree and an artificial potential field. In: Intelligent Robots and Systems 95'. Human Robot Interaction and Cooperative Robots', Proceedings. 1995 IEEE/RSJ International Conference on. IEEE, vol. 2, pp. 474–481.

Kloeden, C.N., McLean, A.J., Glonek, G., 2002. Re-analysis of Travelling Speed and the Rate of Crash Involvement in Adelaide, South Australia. Report CR 207. Australian Transport Safety Bureau, Canberra, Australia.

Li, Q., Zheng, N., Cheng, H., 2004. Springrobot: a prototype autonomous vehicle and its algorithms for lane detection. IEEE Trans. Intellig. Transp. Syst. 5 (4), 300–308.

Lu, G., Chen, B., Lin, Q., Wang, Y., 2012. Quantitative indicator of homeostatic risk perception in car following. Saf. Sci. 50, 1898–1905.

Lu, G., Chen, B., Wang, Y., Lin, Q., 2013. A car-following model based on quantified homeostatic risk perception. Math. Probl. Eng. 2013, 1–13.

Mammar, S., Sébastien, G., Mariana, N., 2006. Time to line crossing for lane departure avoidance: a theoretical study and an experimental setting. IEEE Trans. Intellig. Transp. Syst. 7, 226–241.

McMullin, E., 2002. The origins of the field concept in physics. Phys. Perspect. 4 (1), 13–39.

Neuhaus, F., Dillenberger, D., Pellenz, J., Paulus, D., 2009. Terrain drivability analysis in 3D laser range data for autonomous robot navigation in unstructured environments. In: Emerging Technologies & Factory Automation, ETFA 2009. IEEE Conference on, pp. 1–4.

Ni, D., 2013. A unified perspective on traffic flow theory, part I: the field theory. Appl. Math. Sci. 7 (39), 1929–1946.

Pengfei, Tao, Sheng, Jin, Dianhai, Wang, 2011. Car-following model based on artificial potential field. J. Southeast Univ. (Nat. Sci. Ed.) 4, 038.

Pilutti, T., Ulsoy, A.G., 2003. Fuzzy-logic-based virtual rumble strips for road departure warning systems. IEEE Trans. Intellg. Transp. Syst. 4, 1–12.

Przybyla, Jay, Taylor, Jeffrey, Jupe, Jason, Zhou, Xuesong, 2015. Estimating risk effects of driving distraction: a dynamic errorable car-following model. Transp. Res. Part C 50, 117–129.

Raksincharoensak, P., Akamatsu, Y., Moro, K., et al, 2013. Predictive braking assistance system for intersection safety based on risk potential. Adv. Autom. Control 7 (1), 335–340.

Rimon, E., Koditschek, D.E., 1992. Exact robot navigation using artificial potential functions. IEEE Trans. Robot. Autom. 8 (5), 501–518.

Rossetter, E.J., Gerdes, J.C., 2006. Lyapunov based performance guarantees for the potential field lane-keeping assistance system. J. Dyn. Syst. Meas. Contr. 128 (3), 510–522.

Ruikar, M., 2013. National statistics of road traffic accidents in India. J. Orthop. Traumatol. Rehab. 6 (1), 1.

Schwarz, M., Behnke, S., 2014. Local navigation in rough terrain using omnidirectional height. In: ISR/Robotik 2014; 41st International Symposium on Robotics; Proceedings of. VDE, pp. 1–6.

Suzuki, Shigetaka, Raksincharoensak, Pongsathorn, Shimizu, Ikuko, Nagai, Masao, Adomat, Rolf, 2010. Sensor fusion-based pedestrian collision warning system with crosswalk detection. In: 2010 IEEE Intelligent Vehicles Symposium, University of California, San Diego, CA, USA, June 21–24, TuE1.17.

Tawari, A., Sivaraman, S., Trivedi, M.M., Shannon, T., Tippelhofer, M., 2014. Looking-in and looking-out vision for urban intelligent assistance: estimation of driver attentive state and dynamic surround for safe merging and braking. In: Intelligent Vehicles Symposium Proceedings, 2014 IEEE. pp. 115–120.

Transportation Bureau of the Ministry of Public Security of the PRC, 2014. Annals of Road Traffic Accidents Statistics of the People's Republic of China, Beijing, China (in Chinese).

Van Der Laan, J.D., Heino, A., De Waard, D., 1997. A simple procedure for the assessment of acceptance of advanced transport telematics. Transp. Res. Part C: Emerg. Technol. 5 (1), 1–10.

van Tricht, M.J., Ruhrmann, S., Arns, M., et al, 2014. Can quantitative EEG measures predict clinical outcome in subjects at clinical high risk for psychosis? A prospective multicenter study. Schizophrenia Res. 153 (1), 42–47.

Veelaert, P., Bogaerts, W., 1999. Ultrasonic potential field sensor for obstacle avoidance. IEEE Trans. Robot. Autom. 15 (4), 774–779.

Wang, J., Zhang, L., Zhang, D., Li, K., 2013. An adaptive longitudinal driving assistance system based on driver characteristics. IEEE Trans. Intellg. Transp. Syst. 14, 1–12.

Wang, J., Wu, J., Li, Y., Li, K., 2014. Concept and modeling of driving safety field based on driver-vehicle-road interactions. IEEE 17th ITSC, 974–981.

Wang, Meng, Hoogendoorn, Serge P., Daamen, Winnie, van Arem, Bart, Happee, Riender, 2015. Game theoretic approach for predictive lane-changing and car-following control. Transp. Res. Part C 58, 73–92 (Original Research Article).

Wang, J., Wu, J., Li, Y., 2015. The driving safety field based on driver–vehicle–road interactions. IEEE Trans. Intell. Transp. Syst. 16 (4), 2203–2214.

Ward, James R., Agamennoni, Gabriel, Worrall, Stewart, Bender, Asher, Nebot, Eduardo, 2015. Extending time to collision for probabilistic reasoning in general traffic scenarios. Transp. Res. Part C 51, 66–82.

Warren, C.W., 1990. Multiple robot path coordination using artificial potential fields. In: Robotics and Automation, 1990. Proceedings. 1990 IEEE International Conference on. IEEE, pp. 500–505.

Yiğiter, Özlem, C., Serhan, T., 2014. Lane by lane analysis of vehicle time headways—case study of Izmir ring roads in Turkey. KSCE J. Civ. Eng. 19, 1498–1508.